Jounce Bumper Modelling Using Finite Element Analysis

Mohammed Elmahdi Elgack
Department of Mechanical Engineering
American University of Sharjah
Sharjah, UAE
b00094498@aus.edu

Haret Hossoon
Department of Mechanical Engineering
American University of Sharjah
Sharjah, UAE
b00096464@aus.edu

Omar Ghannam
Department of Mechanical Engineering
American University of Sharjah
Sharjah, UAE
b00094488@aus.edu

Hussien Hussien
Department of Mechanical and Nuclear Engineering
University of Sharjah
Sharjah, UAE
hhussien@sharjah.ac.ae

***Abstract*—Jounce bumpers act as suspension limiters during impact. They prevent the suspension from getting into kinematic singularity situation during shock impacts due to potholes, curbs, and debris on the road. A Jounce bumper is manufactured of hyperplastic materials to make use of the viscoelasticity characteristics allowing it to be a better absorber that minimizes transmitted forces to the vehicle body for failure prevention. Therefore, it is essential to create accurate models for reliable and practical bumpers testing and design optimization before manufacturing. In this work, we will provide a modelling approach to evaluate the static performance of some traditional jounce bumpers. The model accuracy was evaluated using standard bumper tests and found to have a good agreement.**

Keywords—jounce bumper, suspension performance, polyurethane, hyperelastic material model, finite element analysis.

I. INTRODUCTION

Jounce bumpers, also known as "Bump Stops", are essential parts of any automobile suspension system. In cases where wheels are exposed to high dynamic loading from bumps, cracks, as well as other objects on or off the road, these elastic cushions restrict the vertical travel of the suspension system and avert metal-to-metal interaction with the chassis. When the load is at its peak, jounce bumpers can also function as compression springs [1]. The jounce bumper performs many functions, including general load management, ride, and handling, and/or spring assistance [2]. Bumpers' behaviour is typically influenced by the material, form, and density and they come in numerous sizes and shapes, as shown in Fig.1 below [2]. The mechanical behaviour of a jounce bumper when it absorbs a shock is essential not only to prevent potential chassis damage, but it also affects the noise, vibration, and harshness (NVH) performance, which corresponds with the ride quality and passenger comfort.

Fig. 1. Traditional jounce bumpers used in automotive suspension systems [2].

Jounce bumpers are typically designed through a trial-and-error approach. The problem with this approach is the high production cost of prototype moulds, the uncertainty of success, and the time required to alter the prototypes [3]. In this case, the use of computer simulation in the design phase through finite element analysis (FEA) comes in as a very convenient approach. By identifying the bumper material hyperelastic model and experimenting with it using FEA, the number of prototypes required and thus the design cost is minimized [3]. In another approach, a stratification FEA model for the jounce bumper polyurethane (PUR) material is implemented [1]. Using three layers, the stratification principle produces a trustworthy simulation by capturing the actual property distribution in the bumper (skin-transition-core). Optimization of the bumper design is also made easier using FE tools where a dual-rate jounce bumper configuration with improved power management than factory bumpers [4] and a negative Poisson's ratio bumper [5] were explored. In addition, some FEA simulations were performed to evaluate the fatigue life and failure properties of a rubber jounce bumper[6], [7].

This work aims to demonstrate a modelling approach for the jounce bumper's energy absorption (static response) using FEA. Data for the required force-deflection curves will be obtained using Ansys software to cut down the number of required prototypes. Our FEA model results are validated with experiments of actual bumpers and are compared to available works in the literature.

II. HYPERELASTIC MATERIAL MODEL

It is claimed that a material is hyperelastic if it has an elastic strain density function (W), which is a scalar function of the strain deformation tensors and whose derivatives with respect to the strain components determine the corresponding stress components. As a result, the hyperelastic constitutive model has both substantial deformation and material nonlinearity. PUR elastomers that are highly compressible and exhibit hyperelastic material behaviour are typically used for making jounce bumpers. In uniaxial compression, a PUR elastomer's stress-strain relationship is nonlinear; the gradients of the curve rise as the magnitude of the strain does. The Arruda-Boyce model, the neo-Hookean model, the Mooney-Rivlin model, the Marlow model, the polynomial model, the reduced polynomial model, the Yeoh model, the van der Waals model, and the foam model are just a few mathematical representations for hyperelastic materials that are available [1].

A. *Mooney-Rivilin Model*

One well-known empirical model which will be used in this study is the Mooney Rivlin model. The derivatives of the strain energy density with respect to the strain components are used to calculate the stress state for a given strain. The following is the strain energy density function (W) [8]:

$$W = W(\bar{I}_1, I_2, J) = W(\bar{I}_1, \bar{I}_2) + U(J) \quad (1)$$

Where $\bar{I}_1$ and $\bar{I}_2$ are functions of the strain invariants and the determinant of the deformation gradient denoted as J. The strain invariants I_1, I_2, and $I_3 = J^2$ are used to define the strain energy function of the Mooney-Rivlin hyperelastic constitutive model. For a five parameters Mooney-Rivlin model, the strain energy density function is given as [8]:

$$W_{(5)} = C_{10}(\bar{I}_1 - 1) + C_{01}(\bar{I}_2 - 1) + C_{20}(\bar{I}_1 - 1)^2 + C_{01}(\bar{I}_2 - 1)^2 + C_{11}(\bar{I}_1 - 1)(\bar{I}_2 - 1) + \frac{1}{d}(J - 1)^2 \quad (2)$$

Where C_{01}, C_{10}, C_{11}, C_{20} are material constants and d is the compressibility parameter. For the incompressible Mooney-Rivlin model, the corresponding uniaxial stress ($\bar{S}$) is given as [8]:

$$\bar{S}_{5p} = 20C_{10}\left(\lambda - \frac{1}{\lambda}\right) + 2C_{01}\left(1 - \frac{1}{\lambda^3}\right) + 6C_{11}\left(\lambda^2 - \lambda - 1 + \frac{1}{\lambda^2} + \frac{1}{\lambda^3} + \frac{1}{\lambda^4}\right) + 4C_{20}\lambda\left(1 - \frac{1}{\lambda^3}\right)\left(\lambda^2 + \frac{2}{\lambda} - 3\right) + 4C_{02}\left(2\lambda + \frac{1}{\lambda^2} - 3\right)\left(1 - \frac{1}{\lambda^3}\right) \quad (3)$$

For positive definiteness, certain constraints on the Mooney-Rivlin parameters must be met:

$$C_{10} + C_{01} \geq 0,\ C_{20} \geq 0,\ C_{02} < 0 \ and \ C_{20} + C_{02} + C_{11} \geq 0$$

B. *Curve Fitting*

Curve fitting is the process of adjusting a model function's parameters so that the fitted curve closely resembles the measured curve. More than one loading mode should be considered for the fitted model to accurately reflect the actual behaviour of the material. For different hyperelastic models, the curve fitting procedure is the same. It is necessary to derive stress-strain relationships for the identical loading modes that produced the measured stress-strain curves. The stress-strain relations of a 5-parameter polynomial model were derived in basic shear and compression/tension. The three stretch ratios λ_1, λ_2, and λ_3 are used to express the strain invariants [9]:

$$I_1 = \lambda_1^2 + \lambda_2^2 + \lambda_3^2,$$
$$I_2 = \lambda_1^2 \cdot \lambda_2^2 + \lambda_2^2 \cdot \lambda_3^2 + \lambda_3^2 \cdot \lambda_1^2,$$
$$I_3 = \lambda_1^2 \cdot \lambda_2^2 \cdot \lambda_3^2 \quad (4)$$

The stretch ratios λ_i represent a differential cubic volume element's deformation along a Cartesian coordinate system's main axis. The ratio of the distorted length l_i to the undeformed length L_i is employed to define them.

$$\lambda_i = \frac{l_i}{L_i} \quad i \in [1,2,3] \quad (5)$$

Here we obtain the material constants using the uniaxial compression test. While it is necessary to use more than one material response to capture the behaviour accurately, we only expect the bumper to undergo compression so the full material response is not of interest. A rubber block of dimensions 25×25×15 (mm) cut from a PUR jounce bumper of a Mercedes truck strut is tested. Fig.2 shows the material response obtained for the uniaxial compression test.

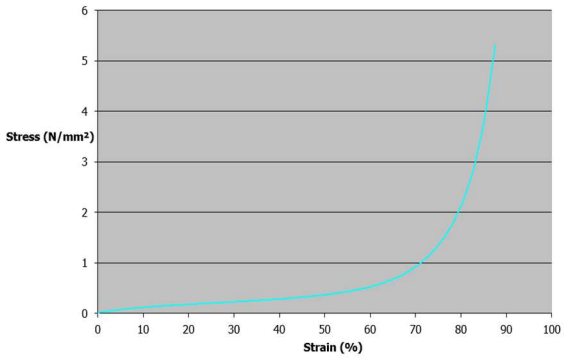

Fig. 2. Uniaxial compression response of a Mercedes PUR bumper.

Ansys have a built-in curve fitting tool which was used to obtain the material constants using the experimental data. However, the tool does not accept inserting the uniaxial compression data only for the curve fitting. This was overcome by inserting the data in Fig.2 in the biaxial tension response as it is identical to the uniaxial compression in terms of the deformation gradient and Anays can accept it as the only response for curve fitting. A 5-parameters Mooney-Rivlin model gave a good fit with a residual of 2.135 Pa. The fitted material response and the corresponding hyperelastic constants are shown below in Fig.3 and Table.I respectively.

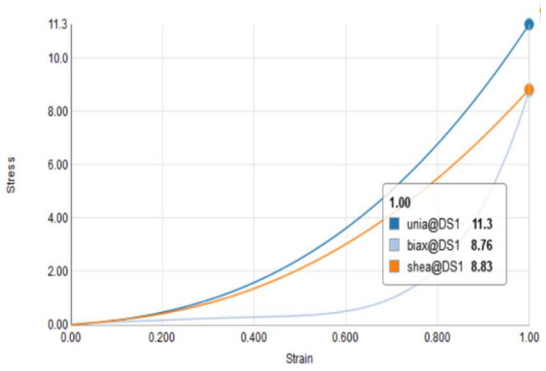

Fig. 3. Material response determined from Ansys curve fitting. The stresses are in MPa.

TABLE I. MOONEY RIVLIN MATERIAL CONSTANTS USED IN THE ANALYSIS.

Mooney-Rivlin Parameters	Values (MPa)
C10	1.0605
C01	-0.85165
C20	0.94865
C11	-0.61812
C02	0.14655

The only missing parameter in the material description is the compressibility parameter d in (2) which needs a volumetric material test. For simplicity, we set the

compressibility to match a constant Poisson's ratio of 0.4. While this might not be the actual case, foam rubbers like PUR exhibit an increase in Poisson's ratio from 0.2-0.3 to near 0.5 at high strains [10] and 0.4 can be considered as an average since the bumper will experience high strains as it is compressed till its solid length.

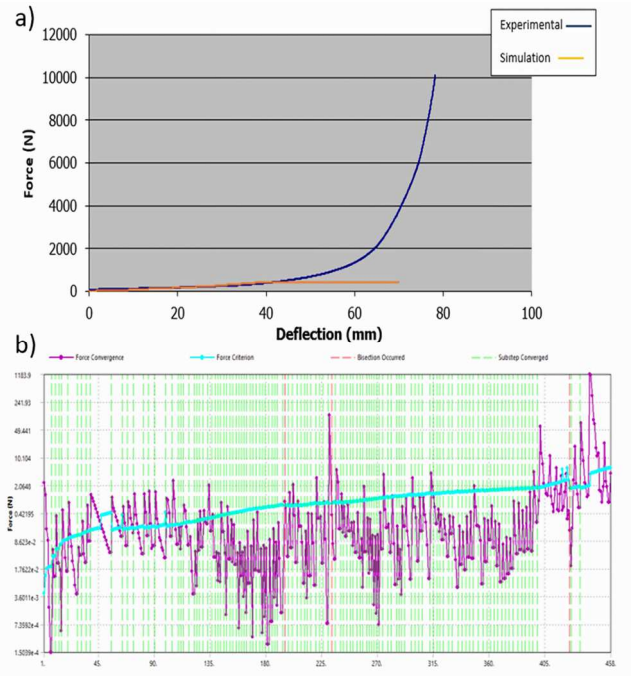

Fig. 4. a) Force deflection curve for a jounce bumper. Although the simulation results from implicit are accurate enough they are useless for the study since they can not describe important features of the bumper response behaviour. b) Forces residuals show the non-convergence even when many equilibrium iterations are performed.

III. Explicit Vs Implicit Approach

There are two approaches to solve time-dependent problems numerically: explicit and implicit. The explicit approach utilizes the current state of the system (initial conditions) to solve for its later states using the Forward Euler method. On the other hand, the implicit approach utilizes the previous states of the system to solve for its current state using the Backward Euler method. The explicit approach requires a smaller time-step increment compared to the implicit approach and that may result in an unstable solution. However, the implicit approach is always stable and it does not require substantially small time increments as the explicit approach does which means that it consumes less computational time. The implicit approach involves either a system of equations to solve or a root-finding technique such as Newton-Raphson, which makes it relatively more complicated to implement from a programming perspective.

As far as our problem is concerned, both explicit and implicit approaches were implemented. Non-convergence issues arise when implementing the implicit approach because of the highly distorted elements, which is expected since the jounce bumper is made of hyperelastic material. The non-convergence happens because of the non-linearities associated with the problem, such as self-contact non-linearity, material non-linearity and geometrical non-linearity. Fig.4a shows the force-deflection curve for the jounce bumper obtained from Ansys using an implicit approach compared to the force-deflection curve obtained from the experiment. The curve obtained from the FEA simulation is identical to the experimental curve until 42 mm of deflection, after that, the simulation curve starts to deviate from the experimental curve. Previous works have used an explicit approach for their jounce bumper simulations to seemingly avoid this problem[4], [5]. All in all, the explicit approach will be used in our work due to the reasons mentioned previously although the implicit approach takes a very short time to solve. With that being said, Fig.4b shows the Newton-Raphson residuals for the force being applied on the jounce bumper. The force represented by the magenta colour is diverging since it can not fall below the force convergence criterion represented by the light blue colour.

IV. Simulation Setup

A. Geometry

An axisymmetric strip of the modelled jounce bumpers, shown in Fig.5, has been drawn using Ansys SpaceClaim. An axisymmetric strip saves computational time dramatically by making use of the jounce bumper symmetrical geometry. It is worth mentioning that the stiffness behaviour of the plates was set as "flexible" since that resolved the contact penetration between the bumper and plate that is experienced when the plates are set to "rigid" stiffness behaviour.

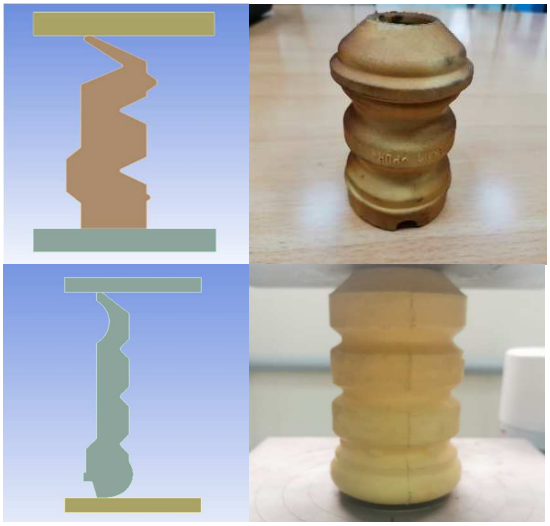

Fig. 5. The traditional jounce bumper that will be used in the analysis are BMW X5 and Mercedes w201 (from top to bottom) both made of PUR. Because of the problem symmetry, an axisymmetric strip of both bumpers is modelled to reduce the computational cost.

B. Contact and Meshing

The jounce bumper will experience contact with both the upper plate and the bottom plate as well as itself. The built-in body interaction tool in explicit is used since it provides robust self-contact capabilities. Trajectory contact detection is used with the penalty formulation. The sliding contact option was set to connected surfaces. Body self-contact was turned on and a friction coefficient of 0.3 was used.

For meshing, explicit physics preference was selected with linear quadrilateral dominant elements. The number of elements was controlled by setting the element size in the bumper to 1 mm. This yielded 1484 elements in the BMW bumper and 1320 elements in the slightly smaller but longer Mercedes bumper. The elemental quality for both meshes was decent as Fig.6 illustrates. The mesh quality is mainly affected by the aspect ratio of the elements which is related to how highly the elements will be distorted while running

the simulation. One represents the highest elements quality while zero represents the lowest. It is clear from the figure that the lowest mesh quality we have is 0.35 and that is the case for two elements only. Most of the elements fall between 0.69 to 0.96 elemental quality which is considered very good.

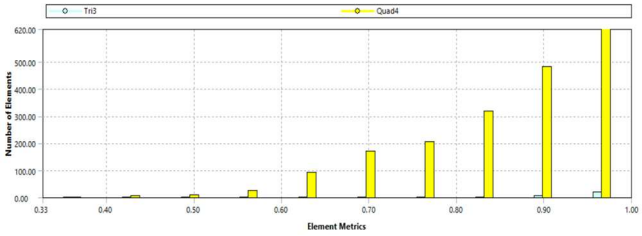

Fig. 6. The mesh quality for the BMW bumper. The other bumper had a similar quality chart.

C. *Boundary and Initial Conditions*

Since the bottom plate is stationary, its displacement was set to zero. The velocity of the upper plate was set to be time-dependent to avoid degrading the elements in the early timesteps. Jounce bumpers standards suggest testing the bumpers at 50 mm/min [1] but this velocity is very slow for the explicit solver. A velocity of 500×time was used, and the density was enlarged 3 orders of magnitude as this accelerate the simulation even more as described by [5]. The validity of the previous approach to obtain an accurate static response of the bumper will be done after the simulations using the energy plots.

V. Results and Discussion

The FE simulations in explicit were able to converge till the compression ended. Fig.7 shows the force-deflection curves of the tested bumpers. From the complete static response, we can observe different bumper behaviours, the initial low stiffness region where the response is almost linear, the hardening region where the bumper reaches the solid length and starts to behave like a rock while the response is getting steeper to eventually reach a high stiffness region. From a vehicle dynamics perspective, we see that both bumpers reach the hardening region approximately at the same time with the BMW one absorbing more energy. This is expected because it is made for a bigger car and has more material in width making it harder to deform. The static response does not show the whole picture of course but it is important for suspension design since more can be deduced if it is used as input for multibody simulations of suspension systems.

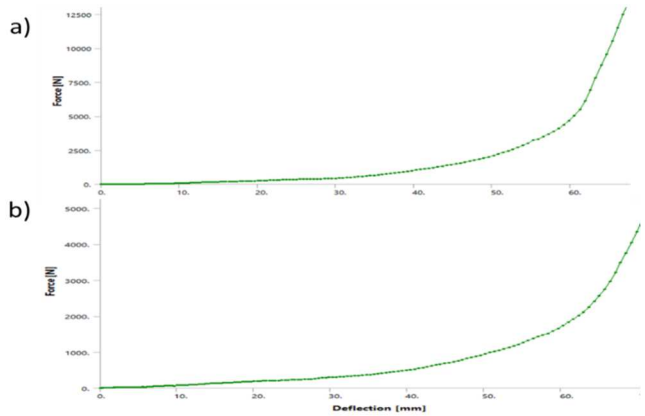

Fig. 7. The static response of both bumpers (a) BMW X5 and (b) Mercedes w201.

To assess the amount of energy error, we plot the total vs kinetic energy of the system which is displayed in Fig.8, and we see that initially the kinetic energy can not be neglected but after the first few time steps, it does not exceed 10% of the total energy of the system except for some point at the end of the first BMW which probably indicates a contact mesh failure and the results beyond these points are not valid.

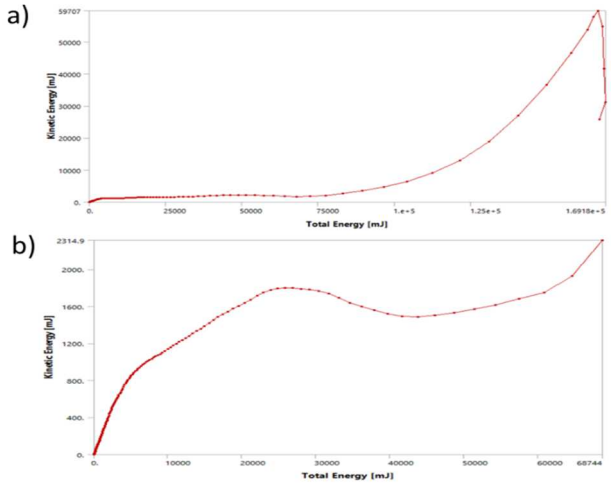

Fig. 8. The energy plots of both bumpers (a) BMW X5 and (b) Mercedes w201.

While 10% inertia might not be small enough to be considered a quasi-static simulation, sample experimental tests can tell us more about the validity of our results. The validation experiments were performed at the standard rate of 50mm/min. We first see that the folding pattern of the bumpers when compared to snapshots of the experiments as seen in Fig.9 is similar meaning that we can capture the physical deformation of the bumper accurately. We also see that both the experimental and FE simulations as seen in Fig.10 are almost identical at the low stiffness region, but they start to deviate slightly when the response reaches the hardening region. Aside from the energy error, this difference can be attributed to the error involved in the curve fitting process from before and the friction effects as demonstrated in [3]. Previous results [1] showed such a deviation as well that keeps increasing for higher deformation. Moreover, they showed that not taking into account the bumper's hard outer layer can lead to a completely underestimated response but we do not see this in our results even though we only modelled the bumper with the core material. All in all, we notice that the difference in our results is comparable to [1], [3] works and the present energy error does not affect the simulations significantly.

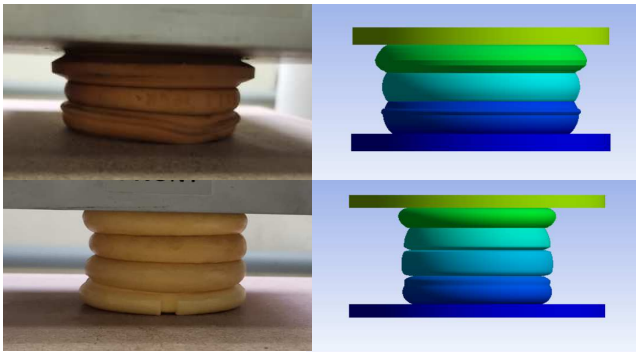

Fig. 9. The bumpers deform with the same pattern as in our FEA model.

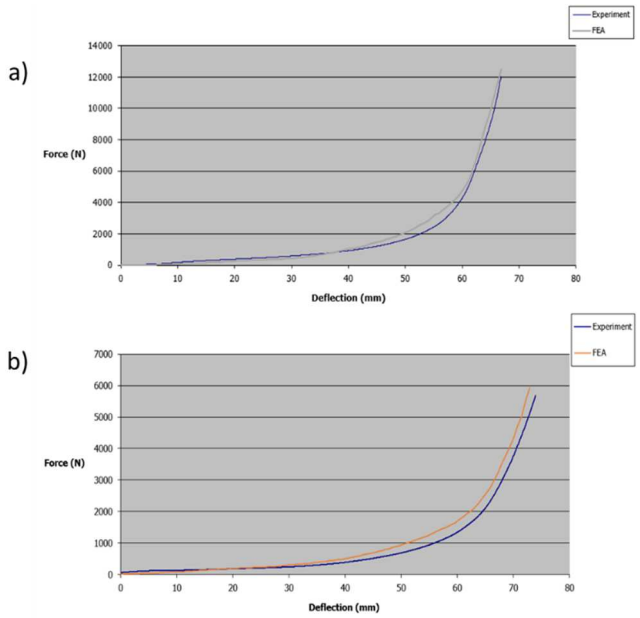

Fig. 10. The experimental validation of the FEA results using the static response for (a) BMW X5 and (b) Mercedes w201 bumpers.

VI. Conclusion

A simple FEA approach to model suspension systems' bump stops was demonstrated. This approach reduces the prototyping costs required for testing. To construct this model one needs to do the following steps:

1) Define the bumper geometry as an axisymmetric slice.
2) Obtain the rubber material constants through curve fitting to a suitable hyperplastic model.
3) Use the explicit solver to perform the simulation and enlarge the density to get an appropriate computational time.
4) Assess the accuracy of the simulation with the energy error and sample experimental data if possible.

It was shown that using only one material response can give satisfactory results for determining the rubber material properties, providing that the fitted quality to the hyperplastic model is good enough. In addition, it was determined that the implicit solver can not converge for the highly non-linear problem and using the explicit solver with some inertia (around 10% in our case) can simulate the bumper static response with good accuracy.

Acknowledgement

The authors would like to thank the American University of Sharjah for providing the computing facilities where the simulations were carried on.

References

[1] Y. Wang, Z. D. Ma, and L. Wang, "A finite element stratification method for a polyurethane jounce bumper," *Proceedings of the Institution of Mechanical Engineers, Part D: Journal of Automobile Engineering*, vol. 230, no. 7, pp. 983–992, Jun. 2016, doi: 10.1177/0954407015602578.

[2] D. Dickson, "A Primer on Jounce Bumper Design Using Microcellular Polyurethane emissions.," in *SAE 2004 World Congress & Exhibition*, 2004. doi: 10.4271/2004-01-1541.

[3] K. Çalışkan, İ. Konukseven, and Y. S. Ünlüsoy, "Product-oriented material testing and FEA for hyperelastic suspension jounce bumper design," *Int. J. Design Engineering*, vol. 3, no. 4, pp. 374–391, 2010, doi: 10.1504/IJDE.2010.040523.

[4] J. A. Schudt, M. Tsai, R. Patil, and R. Geisler, "Dual rate jounce bumper design," in *SAE 2011 World Congress & Exhibition*, 2011. doi: 10.4271/2011-01-0791.

[5] Y. Wang, L. Wang, Z. D. Ma, and T. Wang, "Finite element analysis of a jounce bumper with negative Poisson's ratio structure," *Proc Inst Mech Eng C J Mech Eng Sci*, vol. 231, no. 23, pp. 4374–4387, Dec. 2017, doi: 10.1177/0954406216665415.

[6] M. S. A. Samad, A. Ali, and R. S. Sidhu, "Durability of automotive jounce bumper," *Mater Des*, vol. 32, no. 2, pp. 1001–1005, Feb. 2011, doi: 10.1016/j.matdes.2010.08.017.

[7] A. Ali, R. S. Sidhu, and M. S. A. Samad, "Fatigue Characteristic of Automotive Jounce Bumper," in *New Trends and Developments in Automotive System Engineering*, 2011. doi: 10.5772/12985.

[8] N. Kumar and V. V. Rao, "Hyperelastic Mooney-Rivlin Model: Determination and Physical Interpretation of Material Constants," *MIT International Journal of Mechanical Engineering*, vol. 6, no. 1, pp. 43–46, 2016.

[9] M. Rackl, "Curve Fitting for Ogden, Yeoh and Polynomial Models," in *ScilabTEC Conference*, 2015, pp. 1–11.

[10] B. Sanborn and B. Song, "Poisson's ratio of a hyperelastic foam under quasi-static and dynamic loading," *Int J Impact Eng*, vol. 123, pp. 48–55, Jan. 2019, doi: 10.1016/j.ijimpeng.2018.06.001.